X-ray scattering from warm dense iron

X-ray scattering from warm dense iron

S. White[1], G. Nersisyan[1], B. Kettle[1], T. W. J. Dzelzainis[1], K. McKeever[1], C. L. S. Lewis[1], A. Otten[2], K. Siegenthaler[2], D. Kraus[2], M. Roth[2], T. White[3], G. Gregori[3], D. O. Gericke[4], D.A. Chapman[4,5], K. Wünsch[4], J. Vorberger[6] and D. Riley[1]

[1]*Centre for Plasma Physics, Queen's University Belfast, BT7 1NN, UK*

[2]*Institut für Kernphysik, Technische Universität, DarmstadtD-64289 Darmstadt, Germany*

[3]*Clarendon Laboratory, University of Oxford, South Parks Road OX1 3PU, UK*

[4]*Centre for Fusion, Space and Astrophysics, Department of Physics, University of Warwick, Coventry CV4 7AL, UK*

[5]*Plasma Physics Department, AWE plc, Aldermaston, Reading RG7 4PR, UK*

[6]*Max-Planck-Institut für Physik Komplexer Systeme, 01187 Dresden, Germany*

Abstract

We have carried out X-ray scattering experiments on iron foil samples that have been compressed and heated using laser-driven shocks created with the VULCAN laser system at the Rutherford-Appleton Laboratory. This is the highest Z element studied in such experiments so far and the first time scattering from warm dense iron has been reported. Because of the importance of iron in telluric planets, the work is relevant to studies of warm dense matter in planetary interiors. We report scattering results as well as shock breakout results that, in conjunction with hydrodynamic simulations, suggest the target has been compressed to a molten state at several 100 GPa pressure. Initial comparison with modelling suggests more work is needed to understand the structure factor of warm dense iron.

1. Introduction

The study of warm dense matter (WDM) is of considerable interest due, in large measure, to its relevance to the study of planetary interiors. In such an environment the pressure and temperature can easily reach millions of atmospheres and tens of thousands of Kelvin and there has been debate over the years as to the state of matter under such conditions. For example, whether an element or mixture is solid or liquid, conductive or insulating and what microscopic structure or crystalline state it takes is still a question in the WDM state. In the laboratory we can reproduce such conditions by using, for example, high power lasers to drive a strong shock into a sample. Compression to above solid density and heating to over 10^4 K can ensue. In probing such matter, we have a choice of diagnostics, one of

which is X-ray scattering. This is a powerful diagnostic that has become more widely used in the last decade or so, [e.g. 1-5] because, in principle, it probes the microscopic arrangement of atoms/ions and this itself can be related to bulk properties such as compressibility and conductivity, which are both important parameters in planetary modelling.

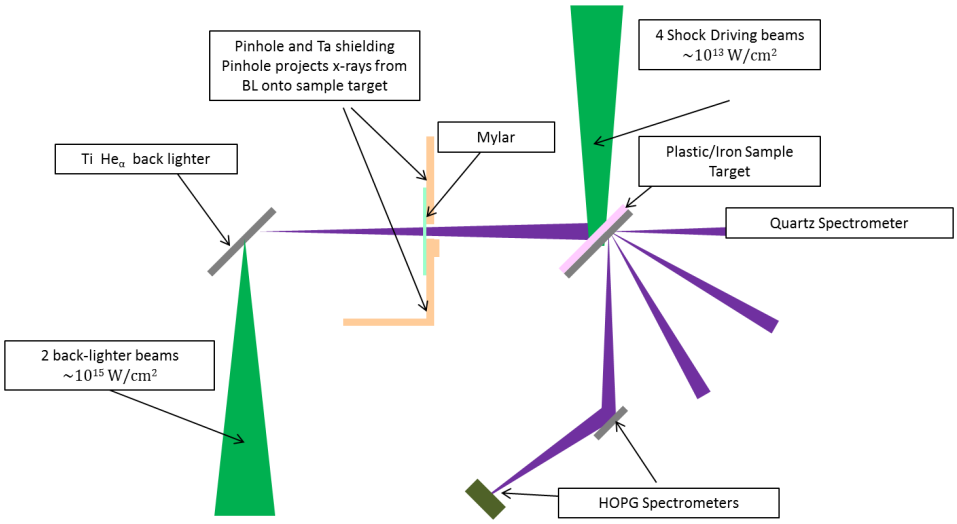

Figure 1 Schematic of experimental arrangement. The distances are not drawn to scale.

X-ray scattering from shock compressed samples has been developed over the past decade and a half to include angularly resolved spectrally integrated scattering [1,6] that explored the ion-ion structure factor and later, spectrally resolved X-ray Thomson scatter [7]. In previous work, a range of materials has been studied that now includes hydrogen [8,9,10], lithium [4,11], beryllium [3], boron [7] and carbon [12] as well as aluminium [1] mixtures such as CH [13] and LiH [14]. In this experiment, we have extended the range to include Fe, an element of primary importance in planetary science due to its abundance in telluric planets.

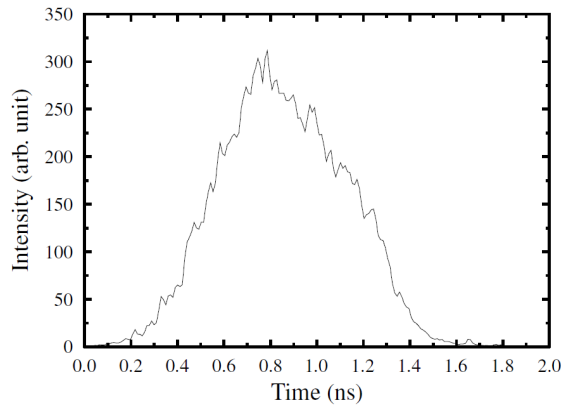

Figure 2. A typical pulse shape measured with optical streak camera.

2. Experiment

The experiment was carried out in Target Area West of the VULCAN laser facility at the Rutherford-Appleton laboratory. A total of 6 beams of approximately 1ns duration were used in second harmonic (wavelength 527nm). In summary, four of the beams were used to drive a strong shock in a foil sample with two further

beams used to create an intense source of X-ray line radiation which back lit the target providing a source of photons for scattering, and as such was referred to as the back-lighter target. The photons scattered from the sample were detected with three different spectrometers consisting of HOPG crystals coupled to CCD detectors. A schematic of the experiment is shown in figure 1.

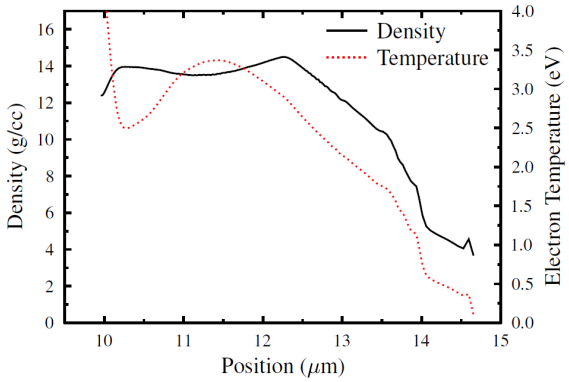

Figure 3 Typical density and temperature conditions for shock compressed Fe at time delay of approximately 0.85ns after start of the shock drive.

The target foil consisted of Fe (7 microns thick) coated, on one side only, with a 6 micron layer of CH. The four shock driving beams were incident in two pairs ±25° above and below the horizontal plane. With the target geometry as shown in figure 1, we have two beams with a 45° incidence and two with approximately 55° degree incidence to normal. The beams were focussed with f/10 lenses and each beam was fitted with a phased zone-plate designed to produce a flat topped focus in an elliptical shape with axes 1.2mm and 1.7 mm. An area of approximately 0.97mm^2 was uniformly illuminated with all four beams overlapping. The typical temporal pulse shape is shown in figure 2. The effective irradiance onto the CH coated side of the target was between 1-3x10^{13} Wcm^{-2}. The CH plays several roles; it helps steepen the shock prior to reaching the Fe, it also reduces X-ray pre-heating and heating by thermal electron conduction in the Fe layer. In figure 3, we show typical conditions predicted to exist in the Fe foil. This prediction was generated using the HYADES [15] simulation code with SESAME [16] equation of state for Fe and CH as well as multi-group diffusion for radiative transfer. The target was simulated using 150 zones for the Fe and 100 for the CH. The ionisation was calculated with a Thomas-Fermi model and cold opacities used at <0.1eV temperature. We can see that there are gradients in density and temperature. Nevertheless, it is also seen that, at this time, a large fraction of the mass remains at a density of between 10 and 14 g/cc and temperature from 2 to 4 eV. As we shall note below, the long pulse duration of the back-lighter means that both temporal and spatial averaging need to be considered.

The two beams used for the back-lighter, were incident in the horizontal plane at 34° and 43° to normal onto a 5 micron thick foil of Ti in order to generate a source of Ti He-alpha photons (1s^2-1s2p ^{1}P and associated satellites) at approximately 4.75keV. The focal spot was ~ 100μm and irradiance approximately 10^{15} Wcm^{-2}. Monitoring of the source with a quartz crystal spectrometer showed that the conversion was routinely between 0.1 and 0.3% of initial laser energy in the He-α line group consisting of the He-like 1s^2-1s2p ^{1}P and 1s^2-1s2p ^{3}P lines as well as Li-like satellites at 4.7-4.75keV. This source was measured on each data shot. The back-lighter foil was placed 7.0mm from the sample

foil centre. The pinhole used to collimate the x-rays was drilled into a 0.5mm Ta plate. The pinhole was 0.75mm diameter and the Ta was bevelled to the edge of the aperture and the effective distance to the back-lighter was 4.0mm. The back-lighter target was oriented at an angle of 30° with respect to the Ta shield, as shown in figure 1. The projected solid angle was ~$3x10^{-2}$ sr and the projected area probed on the sample surface (45° projection) was ~1.3x1.85mm. This was larger than the area where all four shock drive beams overlapped. However, the contribution to scattering from the cold target is measured to be small away from Bragg peaks and could be subtracted from the total scattered signal.

During the experiment a series of "null" shots were taken to ensure that the signal on each

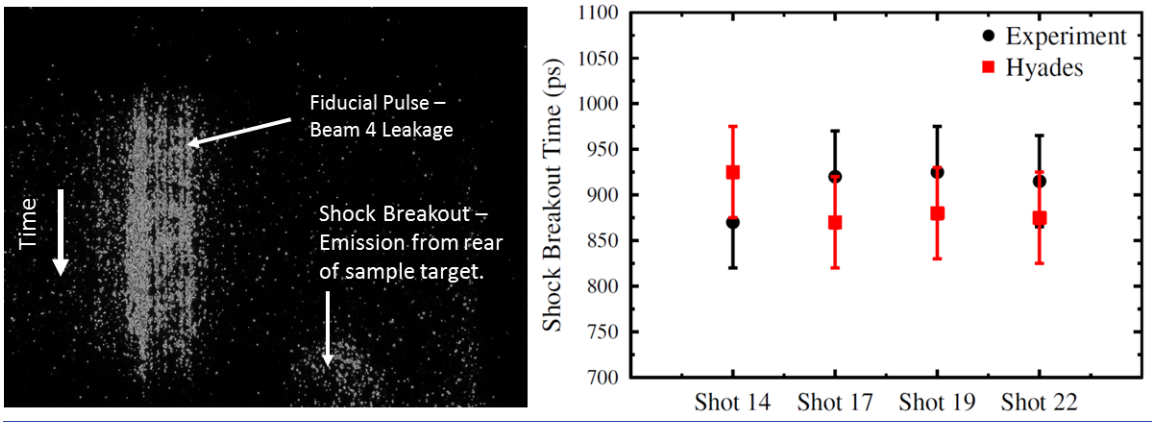

Figure 4 Left: Sample shock breakout data taken with an optical streak camera. The screen is 2ns high in time. Right: Summary of 4 shots showing the differences between measured shock break-out times and simulation based on the measured pulse shape and intensity for each shot.

spectrometer was indeed scatter from the sample and not stray scatter from parts of the sample holder or other sources within the chamber. In addition to this, "cold" shots with just the unshocked sample were taken to ascertain the possible contribution from cold unshocked material. Such shots were taken for cold CH/Fe foils as well as pure CH and Fe foils. As a result of these shots, we are confident that we have signals overwhelmingly from shock compressed Fe in our "full" data shots.

As with many warm dense matter experiments, it is difficult to establish completely independent measurements of density and temperature in the sample. Therefore, we are often, as in this case, dependent on hydrodynamic simulation. As indicated above, we have used the HYADES [15] code to compare shock break-out times between experiment and simulation. The experimental data was taken in a separate series of shots, where the rear surface of the Fe foil was imaged onto the slit of an optical streak camera. The glow from the shock emergence was recorded along with a timing fiducial generated by leakage from a mirror in one of the long pulse beam lines. The timing fiducial was spatially displaced along the streak camera photocathode and timed using light scattered from low energy shots on a diffusive target. In figure 4 we can see some typical data and a summary of

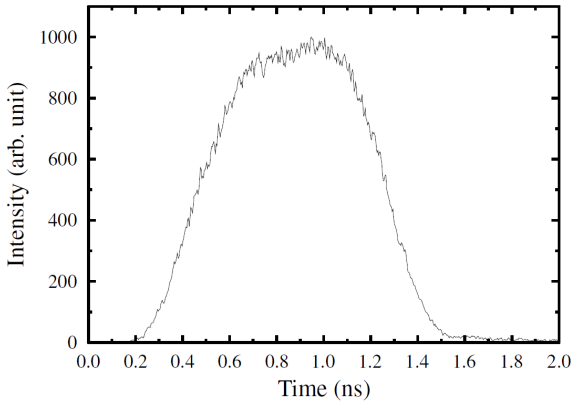

Figure 5. X-ray streak camera data for the He-α back-lighter source on a typical data shot. The back-lighter temporal profile was relatively consistent throughout the experiment.

agreement of experiment and simulation. The agreement is within about 50ps or roughly 5%. This is about the limit of the data resolution, due to both the temporal resolution of the streak camera and the noise in the data. This is not as good as might be obtained in specialised experiments designed to explore equations of state via shock speed measurements. However, since shock pressure, P is expected to scale roughly as $P \sim I^{2/3}$ [17] and shock velocity as roughly $P^{1/2}$, then we can assume that the pressure in the simulations is correct to about 10% and this is not enough to significantly affect our density and temperature profiles, especially when we consider that we are averaging over ~1ns duration of the back-lighter. The main outcome is that we are sure the coated targets are behaving as we expect them to. In the simulation, the shock pressure rises to about 5Mbar (500GPa) with the shock speed in excess of 10 km/s in the Fe. This means that we certainly expect the Fe to melt [18] into a WDM state.

In addition to monitoring the shape of the shock drive beam, the X-ray back-lighter emission was also recorded on each shot with an X-ray streak camera (XRSC) viewing from the top of the chamber and using a HOPG curved crystal (R=115mm) in von-Hamos configuration. The temporal resolution was approximately 100ps, mainly due to slit width and streak rate. In figure 5, we see a typical profile with full width and half maximum (FWHM) of 0.8±0.1ns, which was consistent throughout the experiment despite stronger variations in the optical drive pulse.

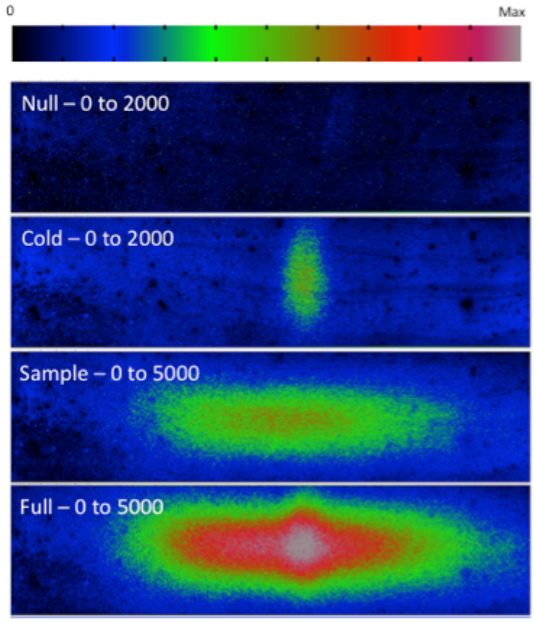

Figure 6 Sample shots showing from top to bottom, a null shot, a cold sample shot, a shock drive only shot and a full scatter shot from a WDM sample. Note the change of scale for the null and cold target shots.

In figure 6 we see a series of data shots of various types taken with the crystal at 38°. The first is a "null" shot to demonstrate a lack of signal in the absence of the sample foil. Note that the empty sample holder was left in place. Cold shots showed weak scatter from the CH layer and this is seen in the second shot from the top.

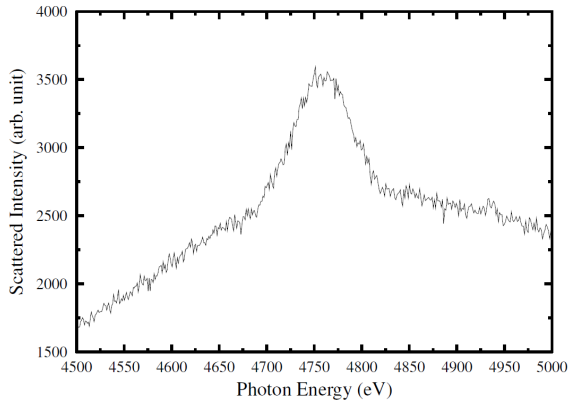

Figure 7. Line out of data shot in figure 6 for HOPG spectrometer which captured scattering at 38°. The scatter signal peak is clearly defined above the background.

For full shots we expect the hot CH plasma to be almost fully ionised and thus scatter even more weakly. The following shot is a shot taken just with the shock drive beams and indicates the level of background radiation from the CH plasma on the front of the target. Finally, we see a "full" shot showing a clear scatter signal above the background.

In figure 7, we can see a line out of the "full" shot. We can see that the background has a bell-like shape. This is due to the effects of the CCD detector plane being aligned so as to intercept the normal to the line focus of the von-Hamos crystal, thus creating a pinch effect where the intensity increases towards the centre of the image where the von-Hamos is in focus. The scatter signal needs to be evaluated by averaging spatially across the width of the CCD. However, we can see from figure 7 that the background is smooth and the signal area well defined.

In calculating the cross-section from the data we have taken into account several factors. Firstly, X-rays at 4.75keV have an attenuation length in cold solid Fe of 8.2 μm. In the forward scatter direction this will not mean that one part of the foil will scatter more than another because the total path through Fe will be the same. However, away from forward scatter it will have an effect and this is accounted for. Secondly, although the incident x-rays are not expected to be polarised, scattering from electrons will induce polarisation in the scattered x-rays. This is important as the HOPG crystal reflectivity is polarisation dependent. The SHADOW extension of the XOP code [19] was used to predict reflectivity of 2.74mrad and 1.64mrad for σ and π incidence respectively and calculated ratios between reflectivity for these cases were used to correct for this effect when considering the data at different scatter angles.

The cross-sections for scattering from a dense plasma can be calculated in units of the differential Thomson scatter cross-section for unpolarised light, $\sigma_{T,}$ [20]. For scatter dominated by the elastic or quasi-elastic features, the scatter cross section is given by;

$$I(k) \approx \sigma_T \left[f_i(k) + q_i(k) \right]^2 S_{ii}(k) = \sigma_T W_R$$

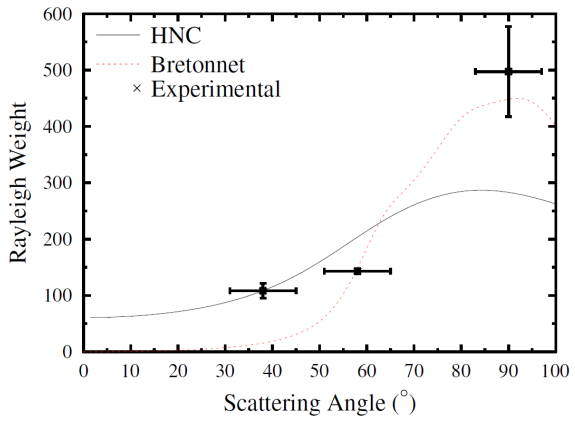

Figure 8. Average cross section in units of the Thomson cross-section from 3 data shots under similar conditions. The horizontal error bars represent the range of angles the HOPG crystals gather over, the vertical error bars are statistical averages over 3 shots.

where k is the scatter wave-vector. The ion-ion structure factor $S_{ii}(k)$ is the Fourier transform of the ion-ion pair distribution function; which reflects the microscopic structure of the plasma which in turn is dependent on the inter-ionic potential. The ionic form factor, $f_i(k)$ and the ion-electron correlation $q_i(k)$ account for the scattering from bound electrons and free electrons correlated to the ion motion, respectively. We call, W_R the Rayleigh weight. The free-electron and bound-free Compton scatter are negligible for this higher Z case.

The shape of the scattering cross-section is determined most directly by $S_{ii}(k)$. We have simulated this for our conditions using two models. First, a hyper-netted chain model with a simple Yukawa type potential is used [21]. The hydrodynamic simulation is divided into three temporal zones, of equal weight as determined from the streak of the back-lighter. At the central point of each time zone, the spatial profile is divided into four slices of equal mass (figure 3 represents the first of these time zones for the data presented below). Thus twelve separate temperature/density combinations are used to average the simulated static structure factor. The same process is repeated using a one-component plasma (OCP) model using the analytical formulation of Bretonnet and Derouiche [22]. We do not expect the unscreened OCP to be valid but is provided as a comparison. In figure 8, we have taken 3 shots under similar conditions. As we can see from figure 8, the error bars due to shot-to-shot variation are small for lower angles of incidence and not too large for 90° scatter ($k \sim 1.7/a_B$ where a_B is the Bohr radius).

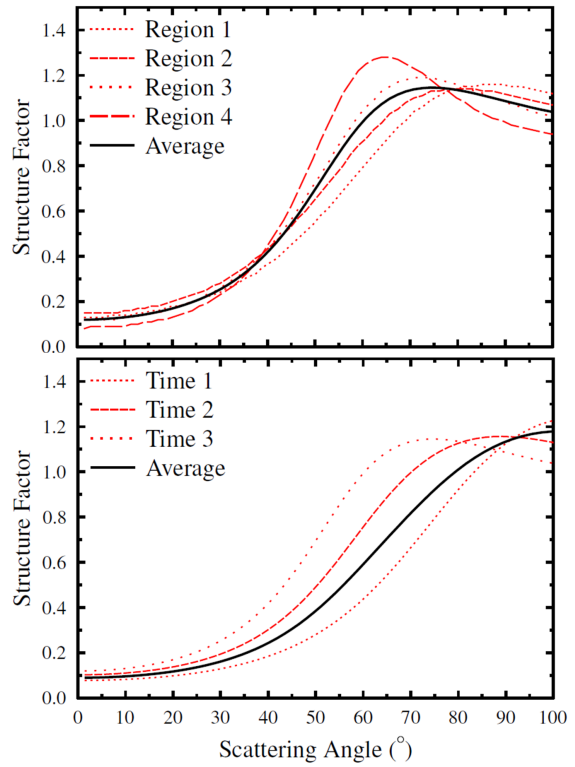

Figure 9 Structure factors from the HNC model. In the top panel we take the average conditions over 4 spatial zones at one time in the simulation. In the lower panel, we use the spatial average conditions for the whole foil but at three times in the simulation.

Although the data clearly indicates a structure factor sharply rising with angle and has reasonable consistency from shot to shot, the comparison with either model does not bring obvious agreement. It is possible that the significant averaging required is the source of disagreement. In figure 9, we can see calculated structure factors $S_{ii}(k)$ using an HNC model for the average conditions in all four spatial regions at one time and also for the spatially averaged conditions at 3 different times. The long back lighter duration leads to uncertainty due to temporal averaging effect.

On the other hand, in order to allow for large numbers of calculations needed in the averaging process, the theoretical models used here are just the basic descriptions leaving out quite a number of physics features that may be important in iron. The principal one is the occurrence of bound electrons forming full shells. These can significantly change the screening properties [23] and the structure factors [24]. Better models should be included in the further analysis.

To be able to successively discriminate between different models describing the structure factors future experiments should address this issue. Experiments of this kind will particularly benefit from the development of hard x-ray free electron laser facilities such as LCLS which can provide over 10^{12} photons at several keV energy in sub-ps pulses at repetition rates in excess of 100Hz [25] allowing one to probe 'snapshots' of the target conditions.

Summary

In this work, we have illustrated X-ray scattering from warm dense Fe. Despite averaging over a back-lighter duration comparable to that of the shock drive, we see a distinct rise with angle in the scatter cross-section, as expected for a strongly coupled warm dense matter state. Comparison with simulation is limited by the need for spatial and temporal averaging and more work is needed with better temporal resolution and more control over the shock drive beams. Nevertheless, this data is encouraging as it indicates that with more evolved experimental design and access to bright shorter pulse back-lighters it should be feasible to obtain good quality scatter data from Fe samples under quite uniform conditions. A dedicated VISAR system on a facility would allow a deeper exploration of the shock drive and perhaps better, more confident, knowledge of the density and temperature. Fe is an important element for planetary and astrophysics and X-ray scatter work on this and alloys relevant to the Earth core will no doubt be pursued further by the present authors and others.

References

1. D Riley, NC Woolsey, D McSherry, I Weaver, A Djaoui, and E Nardi, Phys. Rev. Lett. **84**(8), 1704-1707 (2000)
2. S.H. Glenzer, H.J. Lee, P. Davis, T. Doeppner, R.W. Falcone, C. Fortmann, B.A. Hammel, A.L. Kritcher, O.L. Landen, R.W. Lee, D.H. Munro, R. Redmer, S. Weber, High Energy Density Physics **6**, 1-8 (2010)
3. S. H. Glenzer, G. Gregori, R.W. Lee, F. J. Rogers, S.W. Pollaine, and O. L. Landen,, Phys. Rev. Lett. **90**, 175002 (2003)
4. E. García Saiz, G. Gregori, D.O.Gericke, B. Barbrel, R. J. Clarke, R. R. Freeman, S. H. Glenzer, F. Y. Khattak, M. Koenig, O. L. Landen, D. Neely, P. Neumayer, M. M. Notley, A. Pelka, D. Price, M. Roth, M. Schollmeier, J. Vorberger, R.L. Weber, L. van Woerkom, K. Wünsch and D. Riley, Nature Physics **4**, 940-944 (2008)
5. G. Gregori, S. H. Glenzer, F. J. Rogers, S. M. Pollaine, and O. L. Landen, C. Blancard, G. Faussurier, and P. Renaudin, Phys. Plasmas, **11**(5), 2754 (2004)
6. T. Ma, T. Doeppner, R.W. Falcone, L. Fletcher, C. Fortmann, D. O. Gericke, O. L. Landen, H. J. Lee, A. Pak, J. Vorberger, K. Wünsch, and S. H. Glenzer, Phys. Rev. Lett. **110**, 065001 (2013)
7. P. Neumayer, C. Fortmann, T. Doeppner, P. Davis, R.W. Falcone, A. L. Kritcher, O. L. Landen, H. J. Lee, R.W. Lee, C. Niemann, S. Le Pape, and S. H. Glenzer, Phys. Rev. Lett. **105**, 075003 (2010)
8. K Falk, A P Jephcoat, B J B Crowley, R R Faustlin, C Fortmann, F Y Khattak, A K Kleppe, D Riley, S Toleikis, J Wark, H Wilhelm, G Gregori, J Phys. Conf. Ser. **244**, 0142014 (2010)
9. S.P. Regan, K. Falk, G. Gregori, P.B. Radha, S.X. Hu, T.R. Boehly, B. Crowley, S.H. Glenzer, O.L. Landen, D.O. Gericke, T. Doeppner, D.D. Meyerhofer, C.D. Murphy, T.C. Sangster, and J. Vorberger, Phys. Rev. Lett. **109**, 265003 (2012)
10. K. Falk, S.P. Regan, J. Vorberger, B. Crowley, S.H. Glenzer, S.X. Hu, C.D. Murphy, P.B. Radha, A.P. Jephcoat, J.S. Wark, D.O. Gericke, and G. Gregori, Phys. Rev. E **87**, 043112 (2013)
11. N. L. Kugland, G. Gregori, S. Bandyopadhyay, C. Brenner, C. R. D. Brown, C. Constantin, S. H. Glenzer, F. Y. Khattak, A. L. Kritcher, C. Niemann, A. Otten, J. Pasley, A. Pelka, M. Roth, C. Spindloe and D. Riley, Phys. Rev. E **80**(6), 066406 (2009)
12. A Pelka, G. Gregori, D. O. Gericke, J. Vorberger, S. H. Glenzer, M. M. Günther, K. Harres, R. Heathcote, A. L. Kritcher, N. L. Kugland, B. Li, M. Makita, J. Mithen, D. Neely, C. Niemann, A. Otten, D. Riley, G. Schaumann, M. Schollmeier, An. Tauschwitz, and M. Roth, Physical Review Letters **105** (26), 265701 (2010)
13. B Barbrel, M. Koenig, A. Benuzzi-Mounaix, E. Brambrink, C. R. D. Brown, D. O. Gericke, B. Nagler, M. Rabec le Gloahec, D. Riley, C. Spindloe, S. M. Vinko, J. Vorberger, J. Wark, K. Wünsch and G. Gregori, Phys. Rev. Lett. **102**, 165004 (2009)
14. A.L. Kritcher, P. Neumayer, C. R. D. Brown, P. Davis, T. Doeppner, R.W. Falcone, D. O. Gericke, G. Gregori, B. Holst, O. L. Landen, H. J. Lee, E. C. Morse, A. Pelka, R. Redmer, M. Roth, J. Vorberger, K. Wünsch, and S. H. Glenzer, Phys. Rev. Lett. **103**, 245004 (2009)
15. JT Larsen and SM Lane J. Quant. Spectrosc. Radiat. Transfer **51**, p179 (1994)

16. SP Lyon and JD Johnson JD, Group T-1, Los Alamos National Laboratory Technical Report LA-UR-92E3407 (1992)
17. PC Thompson, PD Roberts, NJ Freeman and PTG Flynn, J.Phys. D**14**, 1215 1981
18. C. S. Yoo, N. C. Holmes, M. Ross, D. J. Webb and C. Pike, Phys. Rev. Lett. **70**, 3931 (1993)
19. M. Sánchez del Río,C. Ferrero and V. Mocella SPIE proceedings vol. **3152**, 148-157 (1997)
20. J. Chihara, J. Phys.: Condens. Matter **12** 231-247 (2000)
21. K. Wünsch, P. Hilse, M. Schlanges, and D. O. Gericke, Phys. Rev. E **77**, 056404 (2008)
22. J. L. Bretonnet and A. Derouiche, Phys Rev B vol **38**(13), p9255 (1988)
23. D. O. Gericke, J. Vorberger, K. Wünsch, G. Gregori, Phys. Rev. E **81,** 065401(R) (2010).
24. K. Wünsch, J. Vorberger, and D. O. Gericke, Physical Review E **79**, 010201(R) (2009).
25. P. Emma, *et al,* Nature Photonics **4,** 641 (2010)